

Studies of the decay $B_s^0 \rightarrow D_s^\mp K^\pm$

B. Storaci* on behalf of the LHCb collaboration

NIKHEF,

Science Park 105, 1098 XG Amsterdam, The Netherlands

**E-mail: Barbara.Storaci@cern.ch*

The decay mode $B_s^0 \rightarrow D_s^\mp K^\pm$ allows for one of the theoretically cleanest time dependent measurements of the CKM angle γ . This contribution reports the world best branching fraction of this decay relative to the Cabibbo-favoured mode $B_s^0 \rightarrow D_s^- \pi^+$ based on data sample of 0.37 fb^{-1} proton–proton collisions at $\sqrt{s} = 7 \text{ TeV}$ collected with the LHCb detector in 2011, resulting in $BR(B_s^0 \rightarrow D_s^\mp K^\pm) = (1.90 \pm 0.12^{stat} \pm 0.13^{syst+0.12f_s/f_d}_{-0.14}) \times 10^{-4}$.

1 Motivation

The least precise direct measured parameter of the unitary triangle is the angle γ . The high abundance of $b\bar{b}$ pairs, together with an excellent proper time resolution, an excellent particle identification and trigger capability to select hadronic final states, allows the LHCb experiment to determine this parameter through a time dependent analysis using the $B_s^0 \rightarrow D_s^\mp K^\pm$ decay. Unlike the flavour-specific decay $B_s^0 \rightarrow D_s^- \pi^+$, the Cabibbo-suppressed decay $B_s^0 \rightarrow D_s^\mp K^\pm$ proceeds through two different tree-level amplitudes of similar strength.

These two decay amplitudes can have a large CP -violating interference via $B_s^0 - \bar{B}_s^0$ mixing, allowing the determination of the CKM angle γ with small theoretical uncertainties through the measurement of tagged and untagged time-dependent decay rates to both the $D_s^- K^+$ and $D_s^+ K^-$ final states¹. Although the $B_s^0 \rightarrow D_s^\mp K^\pm$ decay mode has been observed by the CDF² and BELLE³ collaborations, at present its branching fraction is known with an uncertainty around 23%⁴. Moreover, only the LHCb experiment has both the necessary decay time resolution and access to large enough signal yields to perform the time-dependent CP measurement.

2 The LHCb experiment

The LHCb detector⁵ is a single-arm forward spectrometer covering the pseudo-rapidity range $2 < \eta < 5$, designed for studying particles containing b or c quarks. The detector includes a high-precision tracking system (silicon and straw tube technologies) and a dipole magnet with a bending power of about 4 Tm. The tracking system has a momentum resolution $\Delta p/p$ that varies from 0.4% at 5 GeV to 0.6% at 100 GeV, an impact parameter resolution of $20 \mu\text{m}$ for tracks with high transverse momentum, and a decay time resolution of 50 fs. Charged hadrons are identified using two ring-imaging Cherenkov detectors. Calorimeter and muon systems provide the identification of photon, electron, hadron and muon candidates.

The analysis is based on a sample of pp collisions corresponding to an integrated luminosity of 0.37 fb^{-1} , collected at the LHC in 2011 at a centre-of-mass energy $\sqrt{s} = 7 \text{ TeV}$.

3 Selection

The channels considered as signal in this document are the decays $B^0 \rightarrow D^-\pi^+$, $B_s^0 \rightarrow D_s^-\pi^+$ and the $B_s^0 \rightarrow D_s^\mp K^\pm$. These decays are all characterized by a similar topology and therefore the same trigger, stripping and offline selection are used to select them, minimizing the efficiency corrections.

The LHCb trigger consists of a hardware stage, based on information from the calorimeter and muon systems, followed by a software stage which applies full event reconstruction.

The decays of B mesons can be distinguished from the background by using variables such as the p_T and impact parameter χ^2 of the B , D , and the final state particles with respect to the primary interaction. In addition, the vertex quality of the B and D candidates, the B lifetime, and the angle between the B momentum vector and the vector joining the B production and decay vertices are used in the selection. In order to remove charmless background a requirement in the flight distance χ^2 of the D_s^- from the B_s^0 is applied⁶.

Further suppression of combinatorial backgrounds is achieved using a gradient boosted decision tree technique⁷. The optimal working point is evaluated directly from a sub-sample of $B_s^0 \rightarrow D_s^-\pi^+$ events in data selected using particle identification and trigger requirements. The chosen figure of merit is the significance of the $B_s^0 \rightarrow D_s^\mp K^\pm$ signal, scaled according to the Cabibbo suppression relative to the $B_s^0 \rightarrow D_s^-\pi^+$ signal, with respect to the combinatorial background. Multiple candidates occur in about 2% of the events and in such cases a single candidate is selected at random.

Particle identification (PID) criteria serve two purposes: separate the Cabibbo-favoured from the Cabibbo-suppressed modes (when applied to the bachelor particle) and suppress the misidentified backgrounds which have the same bachelor particle (when applied to the decay products of the D_s^- or D^-). All PID criteria are based on the differences in log-likelihood (DLL) between the kaon, proton, or pion hypotheses. Their efficiencies are obtained from calibration samples of $D^{*+} \rightarrow (D^0 \rightarrow K^-\pi^+)\pi^+$ and $\Lambda \rightarrow p\pi^-$ signals, which are themselves selected without any PID requirements. These samples are split according to the magnet polarity, binned in momentum and p_T , and then reweighted to have the same momentum and p_T distributions as the signal decays under study.

4 Mass fit

The three signal decays are distinguished with particle identification requirements applied at the final stage of the analysis. The signal yields are obtained from extended maximum likelihood unbinned fits to the data. In order to achieve the highest sensitivity, the sample is fitted separately for the magnet up and down data. The signal line shapes are taken from simulated signal events. A mass constraint on the $D_{(s)}$ meson mass is used in order to improve the B mass resolution.

The shape of the signal mass distribution is obtained fitting a double Crystal Ball function which consist of a common Gaussian with two exponential tails, one to describe the radiative tail present in the lower mass region and the other one describing the higher mass region where only the detector resolution is involved.

A common signal shape describes properly both polarities so a simultaneous fit with a common mean and width of the double crystal ball function is used. The mean is free to float in all the fits, while the width is fixed in the B_s^0 -modes from the result obtained in data in the $B^0 \rightarrow D^-\pi^+$ fit corrected for the $B^0 - B_s^0$ differences observed in the simulation samples. The other parameters are fixed from simulation.

Four sources of backgrounds are present: the combinatorial background, the charmless background, the fully reconstructed (misidentified) background and the partially reconstructed back-

ground. The offline selection is optimized to reduce the combinatorial background contribution, and the remaining contamination is fitted with an exponential shape for the modes with a bachelor pion, while it is taken flat for the $B_s^0 \rightarrow D_s^\mp K^\pm$ mode. The validity of this assumption is checked with wrong-side samples and accounted for in the systematic uncertainty associated to the fit model. The other two background categories have different components in the three fits and therefore are explained separately. In all the fits the partially reconstructed background shapes are obtained fitting a non-parametric function on samples of simulated events generated in the specific exclusive modes, corrected for the observed mass shifts, momentum spectra, and particle identification efficiencies observed in data when it is needed. The yields are left free when possible or a gaussian constraint is applied if an expected amount is computable.

In the $B^0 \rightarrow D^-\pi^+$ mass fit the two relevant sources of partially reconstructed background are the $B^0 \rightarrow D^{*-}\pi^+$ and $B^0 \rightarrow D^-\rho^+$ decays and their yields are left free to float in the fit.

In the $B_s^0 \rightarrow D_s^-\pi^+$ mass fit the misidentified $B^0 \rightarrow D^-\pi^+$ shape is fixed from data using a reweighting procedure to account for misidentification momentum dependency⁸. The number of expected events is computed from the yield obtained in the $B^0 \rightarrow D^-\pi^+$ fit and the PID efficiency obtained from calibration sample. Its yield is therefore constrained to this expected value with a 10% uncertainty. The $B^0 \rightarrow D_s^-\pi^+$ yield is calculated based on the $B^0 \rightarrow D_s^-\pi^+$ branching fraction⁴, the measured LHCb value of f_s/f_d ⁹, and the value of the $B_s^0 \rightarrow D_s^-\pi^+$ branching fraction⁶. The shape used is the same of the signal $B_s^0 \rightarrow D_s^-\pi^+$ with the mean position fixed from the $B^0 \rightarrow D^-\pi^+$ fit. The partially reconstructed backgrounds relevant for this fit are the decays $B_s^0 \rightarrow D_s^{*-}\pi^+$ and the $B_s^0 \rightarrow D_s^-\rho^+$. Due to the large correlation between these two components, a gaussian constraint is used for the fraction of these two backgrounds. The fraction is assumed to be the same as in the B^0 case, while the variation is assumed to correspond to 20% $SU(3)$ breaking.

In the $B_s^0 \rightarrow D_s^\mp K^\pm$ mass fit there are numerous reflections which contribute to the mass distribution. The most important reflection is the misidentified $B_s^0 \rightarrow D_s^-\pi^+$ decay. Its shape is fixed from data using the reweighting procedure while the yield is left free to float. The same procedure is also applied on simulation sample to extract the shape of the $B^0 \rightarrow D^-K^+$ misidentified background. The yield is constraint according to the expected $B^0 \rightarrow D^-K^+$ yield corrected for the PID efficiency. In addition, there is potential cross-feed from partially reconstructed modes with a misidentified pion such as $B_s^0 \rightarrow D_s^-\rho^+$, as well as several small contributions from partially reconstructed backgrounds with similar mass shapes. The yields of these modes, whose branching fractions are known or can be estimated are constrained to values obtained based on criteria such as relative branching fractions and reconstruction efficiencies and PID probabilities⁶. The fit results are shown in Fig. 1

5 Systematic uncertainty

Systematic uncertainties related to the fit are evaluated by generating large sets of simulated experiments using the nominal fit, and then fitting them with a model where certain parameters are varied. The sources of systematic uncertainty considered for the fit are signal widths, the slope of the combinatorial backgrounds, and constraints placed on specific backgrounds. The largest deviations are due to the signal widths and the fixed slope of the combinatorial background in the $B_s^0 \rightarrow D_s^\mp K^\pm$ fit. The systematic uncertainty related to PID is evaluated using simulated signal and calibration samples. The observed signal yields are corrected by the difference observed in the (non-PID) selection efficiencies of different modes as measured from simulated events. A systematic uncertainty is assigned on the ratio to account for percent level differences between the data and the simulation. These are dominated by the simulation of the hardware trigger. A total systematic uncertainty of 3.9% for the ratio $B_s^0 \rightarrow D_s^\mp K^\pm / B_s^0 \rightarrow D_s^-\pi^+$, of 3.4% for the ratio $B_s^0 \rightarrow D_s^-\pi^+ / B^0 \rightarrow D^-\pi^+$ and of 4.6% for the ratio $B_s^0 \rightarrow D_s^\mp K^\pm / B^0 \rightarrow D^-\pi^+$ is found.

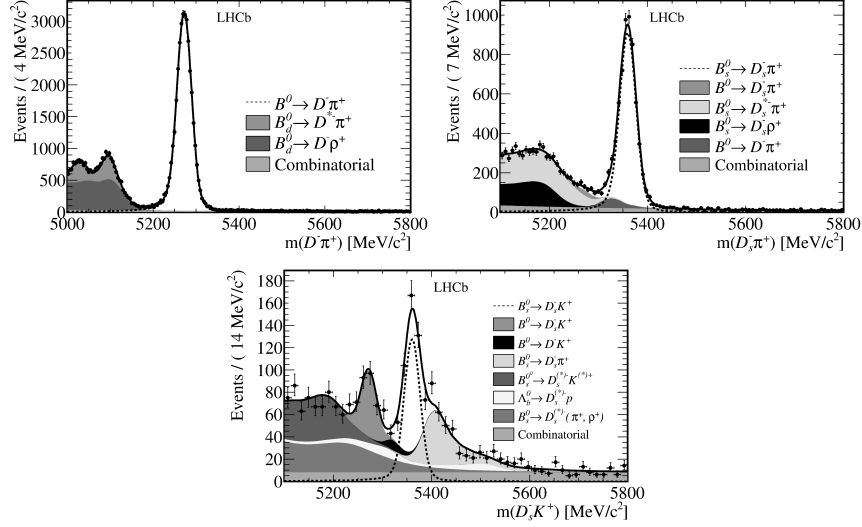


Figure 1: Mass distribution of the $B^0 \rightarrow D^- \pi^+$ candidates (top-left), $B_s^0 \rightarrow D_s^- \pi^+$ candidates (top-right) and $B_s^0 \rightarrow D_s^\mp K^\pm$ (bottom). The stacked background shapes follow the same top-to-bottom order in the legend and in the plot. For illustration purposes the plot includes events from both magnet polarities.

6 Results

The sum of the $B_s^0 \rightarrow D_s^- K^+$ and $B_s^0 \rightarrow D_s^+ K^-$ branching fractions relative to $B_s^0 \rightarrow D_s^- \pi^+$ is obtained by correcting the raw signal yields for PID and selection efficiency differences and it leads to

$$\frac{BR(B_s^0 \rightarrow D_s^\mp K^\pm)}{BR(B_s^0 \rightarrow D_s^- \pi^+)} = 0.0646 \pm 0.0043 \pm 0.0025, \quad (1)$$

where the first uncertainty is statistical and the second is the total systematic uncertainty.

The relative yields of the three decays $B^0 \rightarrow D^- \pi^+$, $B_s^0 \rightarrow D_s^- \pi^+$ and $B_s^0 \rightarrow D_s^\mp K^\pm$ are used to extract the branching fraction of $B_s^0 \rightarrow D_s^- \pi^+$ and $B_s^0 \rightarrow D_s^\mp K^\pm$ together with the recent f_s/f_d measurement from semileptonic decays⁹, leading to

$$BR(B_s^0 \rightarrow D_s^- \pi^+) = (2.95 \pm 0.05 \pm 0.17_{-0.22}^{+0.18}) \times 10^{-3}, \quad (2)$$

$$BR(B_s^0 \rightarrow D_s^\mp K^\pm) = (1.90 \pm 0.12 \pm 0.13_{-0.14}^{+0.12}) \times 10^{-4}, \quad (3)$$

where the first uncertainty is statistical, the second is the experimental systematic plus the uncertainty arising from the $B^0 \rightarrow D^- \pi^+$ branching fraction, and the third is the uncertainty (statistical and systematic) from the semileptonic f_s/f_d measurement. Both measurements are significantly more precise than the existing world averages⁴.

References

1. R. Fleischer, *Nucl. Phys. B* **671**, 0 (2003).
2. T. Aaltonen *et al*, *PRL* **103**, 19 (2009)
3. R. Louvot *et al*, *Phys. Rev. Lett.* **102**, 2 (2009)
4. K. Nakamura *et al*, *J.Phys. G* **37**, 7 (2010)
5. A. A. Alves Jr. *et al*, *JINST* **3**, 8 (2008)
6. R. Aaij *et al*, arXiv:1204.1237v1
7. A. Hoecker *et al*, *PoS ACAT*, 040 (2007)
8. R. Aaij *et al*, *Phys. Rev. Lett.* **107**, 21 (2011)
9. R. Aaij *et al*, *Phys. Rev. D* **85**, 3 (2012)